Journal of Materials Chemistry C

Moderate Temperature Sulfurization and Selenization of Highly Stable Metal Oxides: An Opportunity for Chalcogenide Perovskites

Journal:	*Journal of Materials Chemistry C*
Manuscript ID	TC-COM-07-2023-002716.R1
Article Type:	Communication
Date Submitted by the Author:	26-Sep-2023
Complete List of Authors:	Agarwal, Shubhanshu; Purdue University, Chemical Engineering Turnley, Jonathan; Purdue University, Davidson School of Chemical Engineering Pradhan, Apurva; Purdue University, Chemical Engineering Agrawal, Rakesh; Purdue University,

COMMUNICATION

Moderate Temperature Sulfurization and Selenization of Highly Stable Metal Oxides: An Opportunity for Chalcogenide Perovskites

Shubhanshu Agarwal‡, Jonathan W. Turnley‡, Apurva A. Pradhan, Rakesh Agrawal*

Received 00th January 20xx,
Accepted 00th January 20xx

DOI: 10.1039/x0xx00000x

Oxide perovskites would provide a convenient precursor for the synthesis of chalcogenide perovskites. However, the stability of oxide perovskites means that there is no driving force for sulfurization or selenization with conventional chalcogen sources. In this work, we show that sulfurization and selenization of highly stable early transition metal oxides are possible by heating in the presence of HfH_2 and S or Se, thereby creating HfS_3 or $HfSe_3$ as an oxygen sink and producing an oxygen shuttle in the form of H_2O/H_2S or H_2O/H_2Se. The conversion of ZrO_2 into ZrS_3 or $ZrSe_3$ is supported with thermodynamic calculations and demonstrated experimentally as a proof-of-concept. Subsequently, we demonstrate that $BaZrO_3$ can be converted to $BaZrS_3$ at 575 °C, several hundred degrees below previous methods relying on conventional sulfur sources.

Chalcogenide perovskites are an emerging class of semiconductors that have been proposed as a stable alternative to halide perovskites. These materials have an ABX_3 composition where the A/B cations are in the 2+/4+ or 3+/3+ oxidation states, and the crystal structure is composed of corner-sharing BX_6 octahedra. Chalcogenide perovskites generally contain a sulfide anion; however, select selenide perovskites have been synthesized.[1–3] Most of the known chalcogenide perovskites are made of alkaline earth metals, early transition metals, and metals found in the lanthanide and actinide series.[1,4] Compared with the late-transition metals and post-transition elements that make up many of the traditional semiconductors, the metals that make up chalcogenide perovskites are highly reactive towards oxygen sources and tend to be highly thermodynamically stable as metal oxides.[5,6] Avoiding or bypassing the formation of metal oxides is a significant challenge for synthesizing chalcogenide perovskites and may have contributed to the relatively low number of publications on these materials. In order to make a chalcogenide perovskite, particular thought must be given to precursor selection, chemical handling, and synthesis design.

One route to form chalcogenide perovskites under modest temperatures is to devise a synthesis route that avoids any precursors or intermediates that are highly thermodynamically favorable, particularly metal oxides. As an example, our group has reported solution deposited $BaZrS_3$ and $BaHfS_3$ by using a slurry containing a barium thiolate with ZrH_2 or HfH_2 nanopowders followed by a moderate temperature sulfurization below 575 °C.[7,8] Alternatively, we have also made the same materials using a fully molecular precursor ink containing a barium dithiocarboxylate with a zirconium or hafnium dithiocarbamate followed by a similar sulfurization step.[9] Yang et al. used metal dithiocarbamate precursors to synthesize $BaZrS_3$ nanoparticles at 330 °C in dry oleylamine.[10] Zilevu et al. synthesized $BaZrS_3$ nanoparticles by reacting metal amide precursors with N,N'-diethylthiourea in dry oleylamine at 365 °C.[11] In the case of vacuum deposition, Comparotto et al. sputtered a Ba-Zr layer that was capped with SnS to protect it from oxygen and then used sulfurization at temperatures under 600 °C to volatilize the SnS and produce a $BaZrS_3$ film.[12] Each of these synthesis methods takes advantage of highly reactive precursors to achieve moderate temperature processing. However, this creates other challenges, particularly related to the increased cost of the precursors and the difficulties in handling and storing them due to their reactive nature. Furthermore, thorough removal of O_2 and H_2O during the processing is required to prevent the formation of oxygen-containing secondary phases.

On the other extreme, a common method for making chalcogenide perovskites is to use simple, stable precursors that can be handled in air, followed by conversion to the chalcogenide perovskite phase under extreme conditions. Lelieveld and Ijdo prepared a range of sulfide perovskites by

Davidson School of Chemical Engineering, Purdue University, West Lafayette, Indiana 47907, United States

† Electronic Supplementary Information (ESI) available: [Materials and experimental methods, thermodynamic data and additional calculations, additional XRD and SEM-EDS data, supplementary discussion]. See DOI: 10.1039/x0xx00000x

‡ These authors contributed equally.

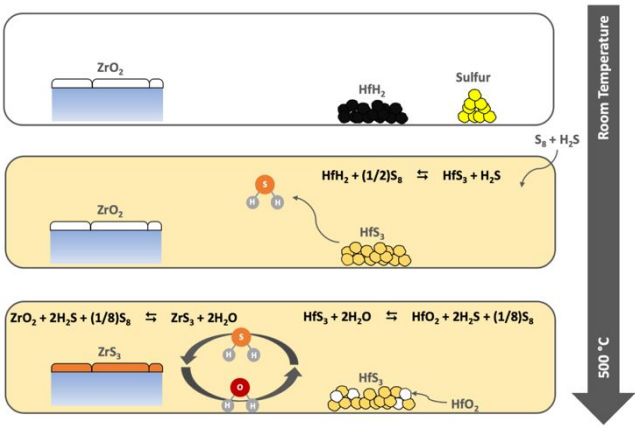

Figure 1. Schematic of proposed sulfurization (or selenization) method where a ZrO_2 film is converted into ZrS_3 (or $ZrSe_3$).

heating alkaline earth carbonates and transition metal oxides in H_2S at 1100 °C for one week.[13] Several groups have produced $BaZrS_3$ by sulfurizing $BaZrO_3$ with CS_2 at temperatures between 900 °C and 1050 °C.[14–17] Alternatively, Márquez et al. and Ramanandan et al. synthesized $BaZrS_3$ thin films by heating an amorphous Ba-Zr-O film to around 1000 °C in the presence of H_2S.[18,19] While there are apparent benefits to developing a synthesis route where most steps do not require careful handling in an inert atmosphere or under vacuum, the temperatures needed to convert oxide precursors into the final chalcogenide perovskite are extremely high. These temperatures are generally incompatible with thin film solar cell fabrication and may even deter further research as not all labs are equipped to work under these conditions.

An ideal route to synthesize chalcogenide perovskites would simultaneously use simple, stable precursors that are easy to handle and leverage thermodynamics to drive the reaction at low-to-moderate temperatures. We propose that this can be done for a range of materials by the sulfurization or selenization of metal oxides in the presence of hafnium hydride, as outlined in Figure 1. In this work we show that the hafnium hydride contributes both an oxygen shuttle in the form of H_2S/H_2O or H_2Se/H_2O and an oxygen sink through the formation of HfO_2, allowing for highly stable metal oxides to be converted to their respective metal chalcogenides at moderate temperatures. Further, we demonstrate that this technique applies to chalcogenide perovskites through the sulfurization of $BaZrO_3$ to produce $BaZrS_3$ below 600 °C, hundreds of degrees below similar oxide-to-sulfide conversions.

To understand the thermodynamics of this oxide-to-chalcogenide conversion, we can start by studying ZrO_2 as a representative system with available thermodynamic data (Table S1 and S2).[20–22] Simple thermodynamic calculations can be done over a range of temperatures with the assumption of constant heat capacity. Depending on which sulfur source is used in excess, ZrS_2 or ZrS_3 can be thermodynamically preferred (Figure S1). However, converting ZrO_2 into a zirconium sulfide is difficult with conventional sulfur sources. As shown in Figure 2a, a reaction of elemental sulfur with ZrO_2 results in a large, positive change in Gibbs energy for the reaction ($\Delta G°_{rxn}$), indicating the reactants are thermodynamically preferred to the

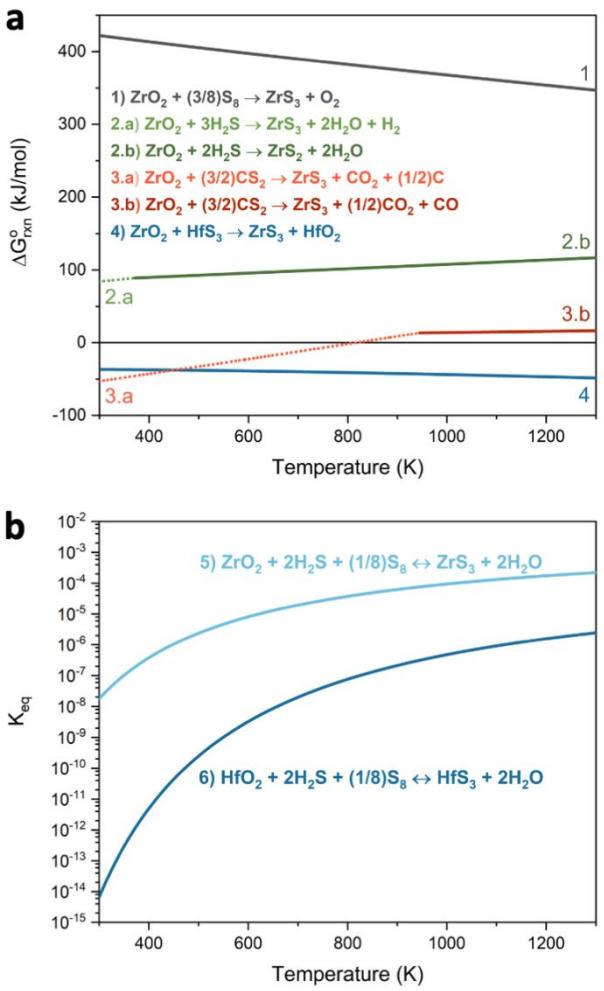

Figure 2. (a) Gibbs Energy of the reaction as a function of temperature and (b) the equilibrium constants as a function of temperature for reactions at the ZrO_2 sample and the HfS_3 oxygen sink with the H_2S/H_2O shuttle.

products.

$$ZrO_2 + (3/8)S_8 \rightarrow ZrS_3 + O_2 \quad (1)$$

Using the more aggressive H_2S as a sulfur source does lower the $\Delta G°_{rxn}$, but it is still a positive value.

$$ZrO_2 + 3H_2S \rightarrow ZrS_3 + 2H_2O + H_2 \quad (2.a)$$

$$ZrO_2 + 2H_2S \rightarrow ZrS_2 + 2H_2O \quad (2.b)$$

With CS_2 as the sulfur source, a negative $\Delta G°_{rxn}$ is obtained around room temperature. However, for this type of conversion, reaction kinetics are often slow until at least moderate temperatures (400-600 °C). At these temperatures, the $\Delta G°_{rxn}$ is near 0 or positive. It should be noted that experimentally CS_2 has been observed to dissociate and form radical starting around 900 °C and this in not captured in these thermodynamic calculations.[23,24]

$$ZrO_2 + (3/2)CS_2 \rightarrow ZrS_3 + CO_2 + (1/2)C \quad (3.a)$$

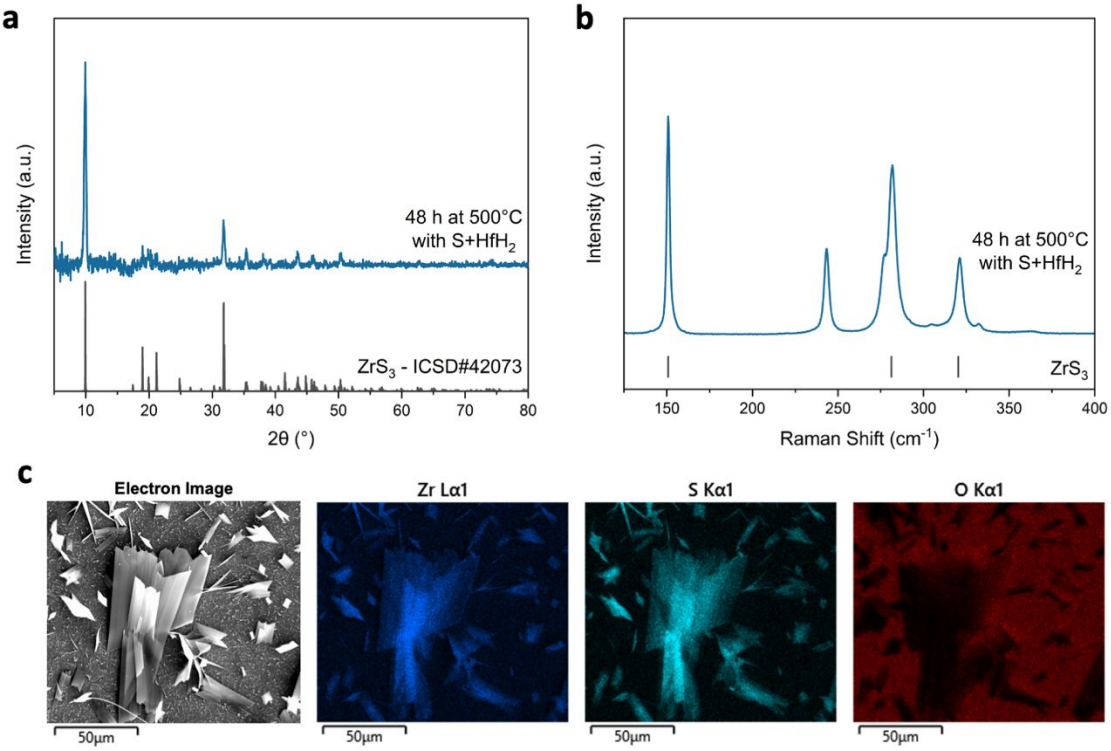

Figure 3. (a) XRD pattern, (b) Raman spectrum, and (c) SEM/EDS images of a sample produced by heating an amorphous ZrO_2 film with HfH_2 and S at 500 °C for 48 h. Reference Raman peak locations were identified by Osada et al.[30]

$$ZrO_2 + (3/2)CS_2 \rightarrow ZrS_3 + (1/2)CO_2 + CO \qquad (3.b)$$

On the other hand, reacting HfS_3 with ZrO_2 to produce ZrS_3 and HfO_2 is favorable as it results in a negative $\Delta G°_{rxn}$. This indicates we could consider HfS_3 a highly aggressive sulfur source for converting metal oxides into metal sulfides.

$$ZrO_2 + HfS_3 \rightarrow ZrS_3 + HfO_2 \qquad (4)$$

However, as HfS_3 is not volatile, it is not a practical sulfur source on its own. So, an additional gas-phase shuttle is needed to shuttle oxygen from the ZrO_2 to the HfS_3 and then return sulfur. This can be achieved in a closed system by heating a ZrO_2 film with HfH_2 and excess sulfur. The sulfur reacts with the HfH_2 to produce HfS_3 and H_2S with excess sulfur remaining. The combination of sulfur and H_2S can then react with the ZrO_2 film. However, the equilibrium position is shifted far to the reactants side of this reaction as indicated by the small K_{eq} shown in Figure 2b.

$$ZrO_2 + 2H_2S + (1/8)S_8 \rightarrow ZrS_3 + H_2O \qquad (5)$$

Notably, the equivalent reaction with HfO_2 has a K_{eq} that is orders of magnitude smaller.

$$HfO_2 + 2H_2S + (1/8)S_8 \rightarrow HfS_3 + H_2O \qquad (6)$$

This means that the HfS_3 will react with the generated H_2O, preventing the reaction at the ZrO_2 sample from ever reaching equilibrium and driving the formation of ZrS_3 via Le Chatelier's Principle.

It should be noted that the boron-chalcogen method has similarly been developed as a method to generate a thermodynamic driving force in converting metal oxides into metal sulfides.[25] In this method a volatile boron chalcogenide reacts with a metal oxide sample to produce the metal sulfide and a solid boron oxide. This method has been successfully applied to chalcogenide perovskites.[26] However, because the oxygen sink is volatile as a chalcogenide and solid as an oxide, an additional purification step is needed post-reaction to remove the formed boron oxide from the matrix of the synthesized metal chalcogenide.

Experimental validation of this hafnium hydride plus chalcogen method was first studied through the sulfurization of ZrO_2 (full experimental methods in the supplemental information). ZrO_2 films were solution processed by coating an ink containing $ZrCl_4$ and ethanol onto alumina-coated EXG glass and heating in air to 300 °C. The resulting films were amorphous ZrO_2. Further heat treatment at 500 °C could be applied to produce a crystalline ZrO_2 sample (Figure S2). ZrO_2 is noted for being chemically inert, and the thermodynamics discussed earlier show why it is difficult to sulfurize. To validate that a simple sulfurization of ZrO_2 is impossible at moderate temperatures, an amorphous ZrO_2 film was heated in an evacuated ampule with sulfur powder to 500 °C for 24 h. As predicted, only crystalline ZrO_2 formed during this heat treatment (Figure S3). On the other hand, treating an amorphous ZrO_2 sample in the presence of HfH_2 and sulfur at 500 °C for 24 h resulted in conversion to ZrS_3 (potentially with a

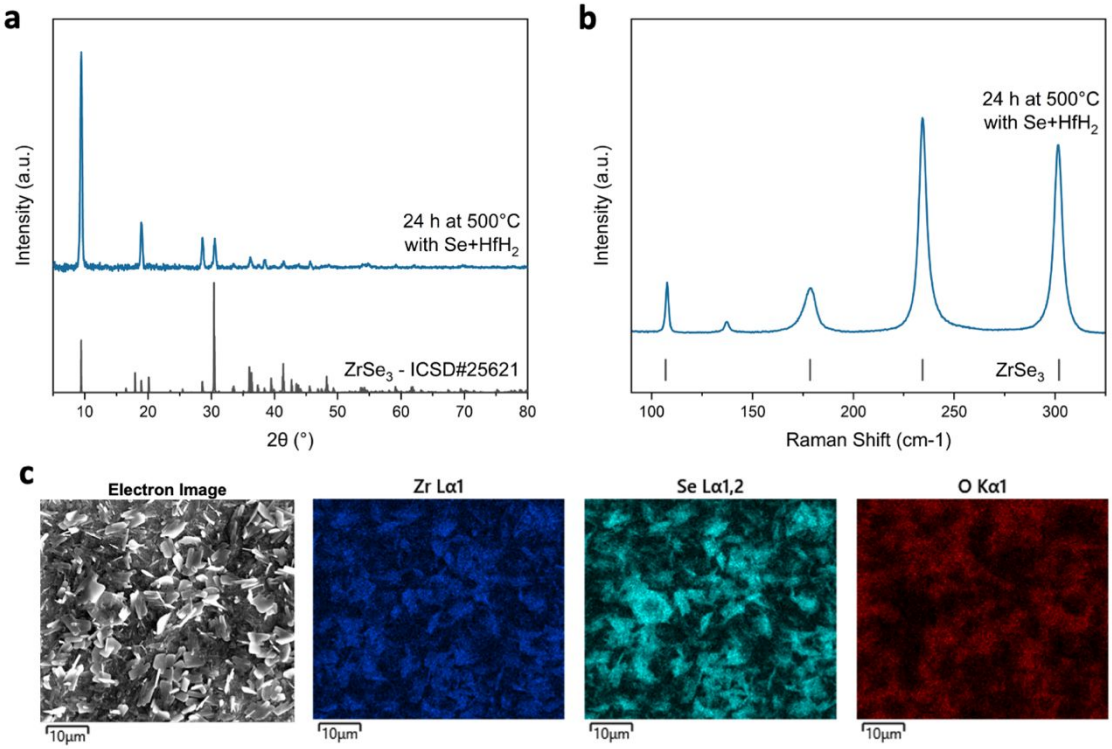

Figure 4. (a) XRD pattern, (b) Raman spectrum, and (c) SEM/EDS images of a sample produced by heating an amorphous ZrO_2 film with HfH_2 and Se at 500 °C for 24 h. Reference Raman peak locations were identified by Osada et al.[30]

small amount of ZrO_2 remaining), confirming the powerful ability of this method for sulfurizing highly stable metal oxides. We also confirmed that the HfH_2 and sulfur react together to generate HfS_3 (Figure S4). A reaction for 48 h convincingly converted all ZrO_2 into ZrS_3. Powder X-ray Diffraction (XRD) results show that all observed peaks can be mapped back to the ZrS_3 sample, though with notable differences in relative intensities (Figure 3a). These intensity differences can be explained by preferential orientation in the sample resulting from the anisotropic nature of the ZrS_3 crystal structure. This transition metal trichalcogenide structure is composed of quasi-1D chains that are bound together into 2D ribbons.[27] These ribbons can then result in preferential orientation with respect to the substrate.[28] Raman Spectroscopy also confirms the formation of ZrS_3, showing the expected peaks at approximately 151, 282, and 321 cm^{-1}. Interestingly, additional peaks are also present, notably at approximately 243 cm^{-1}. This peak is often seen in ZrS_3 samples, and we note that this peak also appears when we measure commercially available ZrS_3 powders.[29] Osada et al. speculated that peaks in this region might arise from defects due to partial surface oxidation.[30] On the other hand, Jin et al. assigned a peak at 244 cm^{-1} to B_g vibrational modes. Further work is needed to assign this peak definitively. Scanning Electron Microscopy (SEM) and Energy Dispersive X-ray Spectroscopy (EDS) also support the XRD and Raman results. In SEM, ribbon structures can clearly be seen, explaining the preferential orientation observed in XRD. Additionally, elemental analysis from EDS shows that the ribbons contain both zirconium and sulfur, while the oxygen signal is only observed where the glass substrate is exposed.

It should be noted that excess sulfur conditions were used, so ZrS_3 was generated. Based on the previously mentioned calculations, lowering the sulfur pressure may allow for formation of ZrS_2 rather than ZrS_3.

Several variations on this sulfurization were performed to clarify the role of the oxygen sink and the oxygen shuttle. First, we studied the importance of the H_2S/H_2O shuttle. By heating the ZrO_2 film in the presence of HfS_2 and sulfur, there is still the same thermodynamic driving force present, but instead of the H_2S/H_2O shuttle, the oxygen and sulfur travel in the gas phase in the form of O_2 and S_8 (smaller sulfur molecules are likely present in small amounts at these reaction temperatures).[31] In this case, the XRD pattern primarily shows the presence of ZrO_2, with just a small peak signaling some formation of ZrS_2 (Figure S5). We also studied the importance of a thermodynamic driving force by heating a ZrO_2 sample in the presence of ZrH_2 and sulfur. As the sample and sink are both zirconium-containing, there is no driving force for oxygen to move from the sample to the sink. If given enough time, oxygen may equilibrate in its distribution between the sample and sink, but when heating to 500 °C for 24 h, only ZrO_2 is observed in the sample (Figure S6). Finally, the thermodynamic calculations presented here suggest that TiH_2 is a viable replacement for HfH_2 in converting ZrO_2 to ZrS_3, though the magnitude of the thermodynamic driving force is reduced with respect to when HfH_2 is used. However, we found that when heating a ZrO_2 sample in the presence of TiH_2 and sulfur, no formation of ZrS_2 or ZrS_3 was observed (Figure S7). The small thermodynamic driving force predicted may be within the error produced by these calculations' simplifying assumptions.

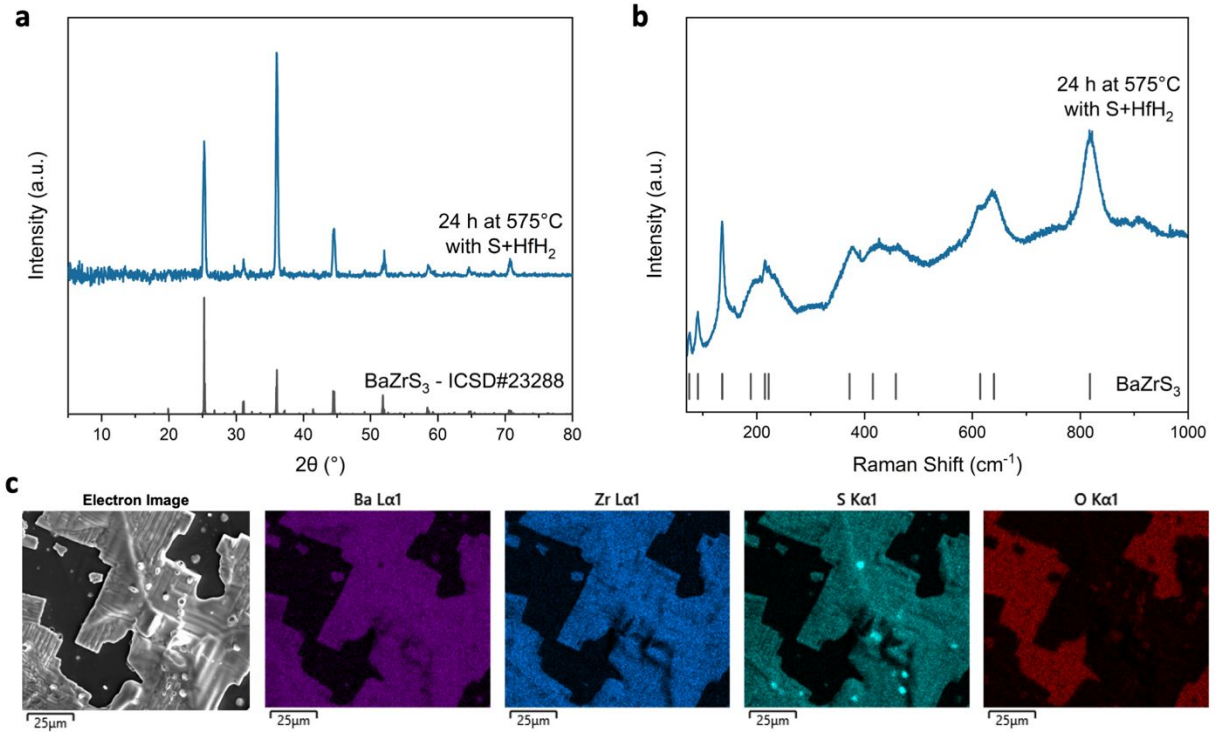

Figure 5. (a) XRD pattern, (b) Raman spectrum, and (c) SEM/EDS images of a sample produced by heating a $BaZrO_3$ film with HfH_2 and S at 575 °C for 24 h. Reference Raman peak locations were identified by Pandey et al.[35]

This method can also be extended to selenization, as exemplified by converting ZrO_2 to $ZrSe_3$ with a $HfSe_3$ sink and an H_2O/H_2Se shuttle. While thermodynamic data for $HfSe_3$ is not available in the literature, we expect an analogous trend as compared to the sulfurization calculations shown in Figure 1. Heating a ZrO_2 film in an evacuated ampule with HfH_2 and selenium powder at 500 °C for 24 h resulted in the formation of $ZrSe_3$. Similarly, XRD shows the formation of oriented $ZrSe_3$ (Figure 4a). As another example of a transition metal trichalcogenide, $ZrSe_3$ is also known to form ribbons, which can lead to preferential orientation. Raman spectroscopy also verifies the presence of $ZrSe_3$ through the observations of peaks at 108, 179, 234, and 301 cm^{-1}. Again, an extra peak is observed at 137 cm^{-1}, which does not match with $ZrSe_2$ or ZrO_2. Further work is needed to determine the identity of this peak, but as is speculated for ZrS_3, it is possibly related to surface defects. SEM/EDS confirms the presence of ribbons that contain both Zr and Se, with oxygen only being observed where the substrate is exposed.

It is important to highlight that not only does this method allow for chalcogenization at moderate temperatures, but it also has significant benefits in reducing the amount of toxic chemicals used. The *in-situ* generation of H_2S or H_2Se means that small quantities on the order of mmol are used and regenerated throughout the chalcogenization. Large-scale storage, handling, and disposal of these toxic gases are not required. Furthermore, flow systems could similarly drive reactions with H_2S or H_2Se by preventing equilibrium gas concentrations from being achieved. But, if there is substantial impurity H_2O concentration in the H_2S/H_2Se source, that could prevent the conversion from taking place. Conversely, unwanted traces of H_2O or O_2 in this system are inherently captured by the oxygen sink, making this method robust towards impurities.

After validating this method by converting binary ZrO_2 into ZrS_3, we turned our attention to the ternary chalcogenide perovskite system by converting $BaZrO_3$ into $BaZrS_3$. Numerous methods have been established for synthesizing $BaZrO_3$ using simple precursors and an air-annealing step, though high temperatures are often needed to achieve crystallinity.[32–34] We synthesized $BaZrO_3$ via solution processing with an ink containing barium acetate, zirconium acetylacetonate, polyvinyl butyral and propionic acid. Following deposition, the film was initially heated at 500 °C for 5 min then at 700 °C for 12 h. This produced a crystalline $BaZrO_3$ material (Figure S8). Sulfurizing this $BaZrO_3$ sample in an evacuated ampule with HfH_2 and sulfur powders produced oxide-free $BaZrS_3$ in 24 h at 575 °C. As shown in Figure 5a, all peaks in the obtained XRD pattern can be mapped back to the $BaZrS_3$ reference, with some degree of preferential orientation. Raman Spectroscopy confirms the formation of $BaZrS_3$ (Figure 5b). SEM/EDS (Figure 5c) shows large patches of material which contain only barium, zirconium, and sulfur. Oxygen is only observed where the substrate is exposed. Though it should be noted that nanoscale domains of secondary phases may not be observed by these characterization methods. Small areas appear to be sulfur-rich, which is likely caused by sulfur condensation on the sample while it is cooling down after sulfurization. This result constitutes a reduction in processing temperature of several hundred degrees compared to previous conversions of $BaZrO_3$ into $BaZrS_3$. Moreover, while this method does use a high-temperature step in producing crystalline $BaZrO_3$, this step is

not necessary, and an amorphous Ba-Zr-O precursor film can be converted to $BaZrS_3$ to keep the entire process at temperatures below 600 °C.

A time study of this conversion (Figures S9-S12) shows no evidence of a gradual transition through a solid-state alloy of crystalline $BaZr(O,S)_3$. The $BaZrO_3$ peaks decrease in intensity and are barely visible in the 4 and 8 h samples. On the other hand, peaks for $BaZrS_3$ start to emerge in the 4 h sample. The observation of clear $BaZrO_3$ and $BaZrS_3$ peaks in XRD is evidence that there is no crystalline $BaZr(O,S)_3$, though there could be amorphous Ba-Zr-O-S phases. This observation is in line with the recent findings of Márquez et al. and Ramanandan et al.[18,19] To further investigate how $BaZrO_3$ is converted to $BaZrS_3$ a 1 h sample was studied, leading to the observation of binary $BaS_4{\bullet}H_2O$ as an intermediate (Figures S13-S15). Altogether, this leads to the interpretation that as the oxygen anions are ripped out of the oxide perovskite, the crystal structure breaks down and the chalcogenide perovskite is formed via a binary-mediated route.

This method need not only be applied when starting with a pure oxide precursor film. In many synthesis methods to date, secondary phases of metal oxides are present in the sulfide material.[18] If chalcogenide perovskite films are made by other methods but have issues with secondary oxide phases, this method could be used to remove the residual oxygen in the material and convert those secondary phases into the desired chalcogenides.

We found that this method could be used to sulfurize other ABO_3 materials. However, there are limitations for certain multinary materials where the sulfurization results in a combination of binary sulfides instead of a multinary sulfide. An example is $SrZrO_3$ (Figure S16). In the case of $BaZrS_3$, a barium polysulfide liquid flux is accessible in this temperature regime and has been shown to facilitate the formation of the ternary sulfide from the binary sulfide, so the same liquid flux might play a role in this synthesis as well.[8,29] This is evidenced by the observation of the barium polysulfide $BaS_4{\bullet}H_2O$, which could indicate a BaS_x liquid flux at higher temperatures. Further discussion on the application of this method for synthesizing other ABS_3 materials can be found in the supplemental information.

In conclusion, careful consideration of thermodynamics can allow for oxide-to-sulfide conversions that are generally unfavorable through the judicious selection of an oxygen shuttle and an oxygen sink. This method has particular relevance to chalcogenide perovskites which have faced many synthesis-related challenges. This work shows that an H_2O/H_2S shuttle with a HfS_3 sink can be created using HfH_2 and sulfur. This method then allows for converting $BaZrO_3$ into $BaZrS_3$ at temperatures below 600 °C, several hundred degrees below similar conversions reported in literature. Therefore, this method allows simple oxide precursors to be used for chalcogenide perovskite synthesis without necessitating excessively high temperatures. Furthermore, this method can be translated to other material systems with a straightforward consideration of the thermodynamics.

Conflicts of interest

There are no conflicts to declare

Acknowledgements

The authors are grateful for the financial support from the National Science Foundation through Grants 1735282-NRT (SFEWS) and 10001536 (INFEWS). We would also like to thank Kiruba Catherine Vincent and Daniel Hayes for their insightful discussions.

References

1 K. V. Sopiha, C. Comparotto, J. A. Márquez and J. J. S. Scragg, *Adv. Opt. Mater.*, 2022, **10**, 2101704.

2 H. Zhang, X. Wu, K. Ding, L. Xie, K. Yang, C. Ming, S. Bai, H. Zeng, S. Zhang and Y.-Y. Sun, *Chem. Mater.*, 2023, **35**, 4128–4135.

3 I. Sadeghi, K. Ye, M. Xu, Y. Li, J. M. LeBeau and R. Jaramillo, *Adv. Funct. Mater.*, 2021, **31**, 2105563.

4 D. Tiwari, O. S. Hutter and G. Longo, *J. Phys. Energy*, 2021, **3**, 034010.

5 K. P. Kepp, *Inorg. Chem*, 2016, **55**, 9461–9470.

6 D. Zilevu and S. E. Creutz, *Chem. Commun.*, 2023, **59**, 8779–8798.

7 J. W. Turnley, K. Catherine Vincent, A. A. Pradhan, I. Panicker, R. Swope, M. C. Uible, S. C. Bart and R. Agrawal, *J. Am. Chem. Soc.*, 2022, **144**, 18234–18239.

8 K. C. Vincent, S. Agarwal, J. W. Turnley and R. Agrawal, *Adv. Energy Sustain. Res.*, 2023, **4**, 2300010.

9 A. A. Pradhan, M. C. Uible, S. Agarwal, J. W. Turnley, S. Khandelwal, J. M. Peterson, D. D. Blach, R. N. Swope, L. Huang, S. C. Bart and R. Agrawal, *Angew. Chemie - Int. Ed.*, 2023, **62**, e202301049.

10 R. Yang, A. D. Jess, C. Fai and C. J. Hages, *J. Am. Chem. Soc.*, 2022, **144**, 15928–15931.

11 D. Zilevu, O. O. Parks and S. E. Creutz, *Chem. Commun*, 2022, **58**, 10512–10515.

12 C. Comparotto, P. Ström, O. Donzel-Gargand, T. Kubart and J. J. S. Scragg, *ACS Appl. Energy Mater.*, 2022, **5**, 6335–6343.

13 R. Lelieveld and D. J. W. Ijdo, *Acta Crystallogr.*, 1980, **B36**, 2223–2226.

14 A. Clearfield, *Acta Crystallogr.*, 1963, **16**, 135–142.

15 S. Perera, H. Hui, C. Zhao, H. Xue, F. Sun, C. Deng, N. Gross, C. Milleville, X. Xu, D. F. Watson, B. Weinstein, Y. Y. Sun, S. Zhang and H. Zeng, *Nano Energy*, 2016, **22**, 129–135.

16 N. Gross, Y. Y. Sun, S. Perera, H. Hui, X. Wei, S. Zhang, H. Zeng and B. A. Weinstein, *Phys. Rev. Appl.*, 2017, **8**, 044014.

17 X. Wei, H. Hui, C. Zhao, C. Deng, M. Han, Z. Yu, A. Sheng, P. Roy, A. Chen, J. Lin, D. F. Watson, Y. Y. Sun, T. Thomay, S. Yang, Q. Jia, S. Zhang and H. Zeng, *Nano Energy*, 2020, **68**, 104317.

18 J. A. Márquez, M. Rusu, H. Hempel, I. Y. Ahmet, M.

Kölbach, I. Simsek, L. Choubrac, G. Gurieva, R. Gunder, S. Schorr and T. Unold, *J. Phys. Chem. Lett.*, 2021, **12**, 2148–2153.

19 S. P. Ramanandan, A. Giunto, E. Z. Stutz, B. Reynier, I. T. F. M. Lefevre, M. Rusu, S. Schorr, T. Unold, A. Fontcuberta I Morral, J. A. Márquez and M. Dimitrievska, *J. Phys. Energy*, 2023, **5**, 014013.

20 J. R. Rumble Jr., D. R. Lide and T. J. Bruno, Eds., *CRC Handbook of Chemistry and Physics*, CRC Press, Boca Raton, RL, 98th edn., 2017.

21 K. C. Mills, *Thermodynamic Data for Inorganic Sulphides, Selenides and Tellurides*, The Butterworth Group, London, 1974.

22 P. L. Brown, E. Curti and B. Grambow, *Chemical Thermodynamics of Zirconium*, OECD Nuclear Energy Agency, 1st edn., 2005.

23 T. C. Peng, *J. Phys. Chem.*, 1974, **78**, 634–638.

24 Z. Yu, X. Wei, Y. Zheng, H. Hui, M. Bian, S. Dhole, J. H. Seo, Y. Y. Sun, Q. Jia, S. Zhang, S. Yang and H. Zeng, *Nano Energy*, 2021, **85**, 105959.

25 L. S. Breton, V. V Klepov and H.-C. Zur Loye, *J. Am. Chem. Soc.*, 2020, **142**, 16.

26 R. Bystrický, S. K. Tiwari, P. Hutár, L. Vančo and M. Sýkora, *Inorg. Chem.*, 2022, **61**, 18823–18827.

27 J. O. Island, A. J. Molina-Mendoza, M. Barawi, R. Biele, E. Flores, J. M. Clamagirand, J. R. Ares, C. Sánchez, H. S. J. van der Zant, R. D'Agosta, I. J. Ferrer and A. Castellanos-Gomez, *2D Mater.*, 2017, **4**, 022033.

28 C. F. Holder and R. E. Schaak, *ACS Nano*, 2019, **13**, 7359–7365.

29 R. Yang, J. Nelson, C. Fai, H. Arif Yetkin, C. Werner, M. Tervil, A. D. Jess, P. J. Dale and C. J. Hages, *Chem. Mater.*, 2023, **35**, 4743–4750.

30 K. Osada, S. Bae, M. Tanaka, H. Raebiger, K. Shudo and T. Suzuki, *J. Phys. Chem. C*, 2016, **120**, 4653–4659.

31 H. Rau, T. R. N. Kutty and J. R. F. Guedes de Carvalho, *J. Chem. Thermodyn.*, 1973, **5**, 833–844.

32 T. Gupta, D. Ghoshal, A. Yoshimura, S. Basu, P. K. Chow, A. S. Lakhnot, J. Pandey, J. M. Warrender, H. Efstathiadis, A. Soni, E. Osei-Agyemang, G. Balasubramanian, S. Zhang, S. F. Shi, T. M. Lu, V. Meunier and N. Koratkar, *Adv. Funct. Mater.*, 2020, **30**, 2001387.

33 S. Sharma, Z. Ward, K. Bhimani, K. Li, A. Lakhnot, R. Jain, S.-F. Shi, H. Terrones and N. Koratkar, *ACS Appl. Electron. Mater*, 2021, **3**, 3306–3312.

34 T. Schneller and T. Schober, *Solid State Ionics*, 2003, **164**, 131–136.

35 J. Pandey, D. Ghoshal, D. Dey, T. Gupta, A. Taraphder, N. Koratkar and A. Soni, *Phys. Rev. B*, 2020, **102**, 205308.